Synthesis of ZnO nanorods modified with TPP, TPPS and Cu-TPPS for photodegradation of MB

Rahmatollah Rahimi*, Javad Shokrayian, Mahboubeh Rabbani

Department of Chemistry, Iran University of Science and Technology, Narmak, Tehran 16846-13114, Iran

E-mail: Rahimi_rah@iust.ac.ir

Abstract

In this study, ZnO nanorods have been synthesized by a simple precipitation technique with zinc nitrate as starting material in the presence of ammonium hydroxide followed by calcination at 450 ˚C. Then meso-tetrakis(4-phenyl) porphyrin (TPP), meso-tetrakis(4-sulfonatophenyl) porphyrin (TPPS), and Copper meso-tetrakis(4-sulfonatophenyl) porphyrin (Cu-TPPS) have been immobilized on the ZnO nanorods and the potential of the obtained photocatalysts in degradation of methylene blue dye was studied under UV and visible irradiation. The photocatalysts were characterized by various techniques such as XRD, SEM and FT-IR. The influence of experimental parameters on the dye photodecolorization process was studied. The role of porphyrins as sentisizers was also investigated on decolorization rate. Under these optimum conditions, the obtained decolorization efficiency for MB dye was more than 90% under visible light. The reusability of the intended catalyst was also investigated.

ZnO nanorod

Keywords: ZnO nanorods, TPPS, Porphyrin**,** Photocatalyst, Methylene blue.

1. Introduction

Semiconductors such as ZnO and TiO_2 have a filled valence band and an empty conduction band and therefore can act as sensitizers for light-reduced redox processes [1]. Among semiconductors, ZnO is a very common material with excellent chemical and thermal stability [2]. It can provide high mobility [3], high transparency [4], nontoxicity and biocompatibility [5]. According to great function of zinc oxide, several techniques have been proposed for zinc oxide synthesis such as thermal decomposition method [5,6], hydrothermal synthesis [4,7], sol–gel synthesis [8], flame

spray pyrolysis [9] and precipitation method [10]. Since environmental problems such as water pollution, semiconductor based photocatalytic reactions have attracted interest as an effective candidate for purifying contaminants [11]. The most efficient materials for photocatalytic applications are semiconductor oxides on nanoscale. Furthermore, shape of accumulation of crystals, have an important role in its applications [8], because the electrical and optical properties of nanomaterials depend on both size and shape of the particles. Therefore, it is desired to synthesize nanomaterials in a simple method which both shape and size factors can be controllable. For zinc oxide particles, various shapes including nanorods [11,12], whiskers [13,14] and nanowires [15] have been successfully prepared.

Many studies on the performance of ZnO particles as Photocatalyst have been performed to remove contaminants [14-16]. It is known that the solar spectra usually contain about 4% UV light. Therefore, pure ZnO, with large direct band gap energy of 3.37 eV at room temperature, cannot make use of the solar spectra efficiently [4]. To overcome this problem, several approaches have been proposed in the literature in which the response of the semiconductor was extended towards the visible region. Among them, dye sensitization has been widely used in order to extend the absorption range to the visible region [17].

In this paper, we synthesized ZnO nanorods by a simple method (without any surfactant) and after that meso-tetrakis(4-phenyl) porphyrin (TPP), meso-tetrakis(4-sulfonatophenyl) porphyrin (TPPS) and copper meso-tetrakis(4-sulfonatophenyl) porphyrin (Cu-TPPS) have been immobilized on surface of ZnO nanorods. Then the photocatalytic degradation of MB on TPP/ZnO, TPPS/ZnO, Cu-TPPS/ZnO and ZnO nanorods was investigated under ultraviolet and visible light.

2. Experimental

2.1. Materials and Methods

All of the Chemicals used in this work were analytical grade reagents and used without further purification. Zinc nitrate ($Zn(NO_3)_2.6H_2O$) , ammonia (25%), pyrrole, propionic acid, benzaldehyde and sulfuric acid were purchased from Merck company. Deionized water was used to prepare all solutions.

The samples were characterized by X-ray powder diffraction (XRD) using JEOL X-ray diffractometer with Cu Kα radiation. The particle morphologies of the ZnO powder were

observed by an AIS2100 (Seron Technology) scanning electron microscopy (SEM). The FT-IR analyses were carried out on a Shimadzu FTIR-8400S spectrophotometer using a KBr pellet for sample preparation. DRS spectra were prepared via a Shimadzu (MPC-2200) spectrophotometer.

2.2. Preparation of copper meso-tetrakis(4-sulfonatophenyl) porphyrin (TPPS)

10 mmol of freshly distilled pyrrole (0.7 ml), 10 mmol of benzaldehyde, 100 ml of propionic acid and 15 ml of nitrobenzene were added to a 250 mL flask. The mixture was allowed to reflux under stirring at 120 ˚C for 60 min. After that, the resulting mixture was cooled overnight in room temperature and filtrated under reduced pressure. The crude product was purified by column chromatography (Silica gel, chloroform/ethyl acetate = 20:1 as an eluent) and a desired purple solid of meso-tetrakis(phenyl) porphyrin (TPP) was obtained (30%).

For synthesis of meso-tetrakis(4-sulfonatophenyl) porphyrin (TPPS), 0.2 g of TPP was dissolved in 5 ml of concentrated H_2SO_4 (Scheme 1). The mixture was heated in a steam bath for 4 h then allowed to stand for 48 h. The resulting solution was neutralized by NaOH (3N) and then the solvent was removed under vacuum at room temperature. The product was washed with methanol until no TPPS could be detected in the solution by UV–visible spectrophotometer.

For synthesis of copper meso-tetrakis(4-sulfonatophenyl) porphyrin (Cu-TPPS), 1mmol of TPPS and 2 mmol $Cu(NO_3)_2.3H_2O$ was dissolved in 20 ml of DMF. The mixture was refluxed for 4 h then allowed to stand for 48 h.

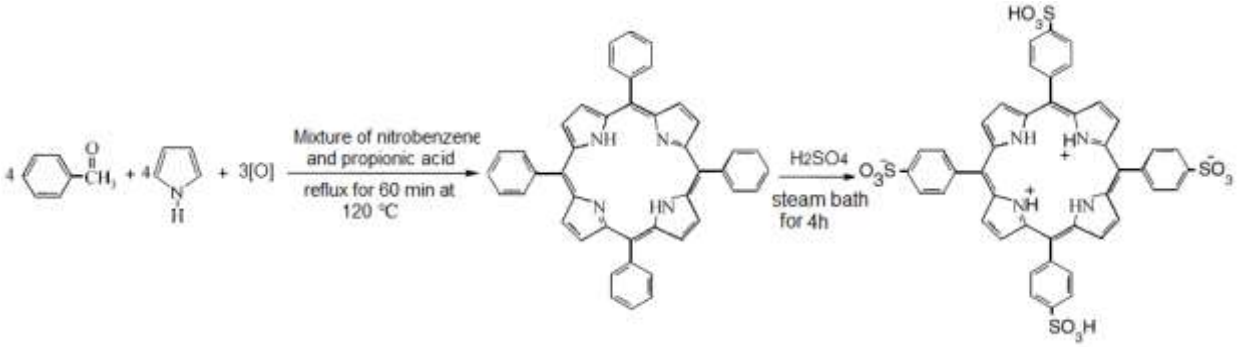

Scheme 1. Synthesis of the meso-tetrakis(4-sulfonatophenyl) porphyrin (TPPS).

2.3. Preparation of ZnO nanorods

5.94 g of $Zn(NO_3)_2.6H_2O$ was added to 500 ml distilled water to obtain a concentration of 0.04 M. The ammonia solution (25%) was added dropwise to solution to achieve pH=11, then the solution was refluxed under stirring. The white precipitation was deposited in the bottom of the

flask. Finally, the mixture was centrifuged and the white solid was collected and washed with distilled water. The obtained solid was dried at 100 ˚C under oven for 3 h, followed by calcination at 450 ˚C for 3 h.

2.4. Modification of ZnO nanorods by porphyrins

0.02 mmol of TPP, TSPP or Cu-TPPS was dissolved in 50 ml of H_2O and 0.02 mmol of finely grounded ZnO nanorods (2 mg) was added to this solution. The resulting suspension was stirred under refluxing for 5 h and then the solvent was removed under vacuum at room temperature. The resulting solution was cooled in room temperature for 24 h. Consequently, the product was washed with ethanol until no porphyrin could be detected in the supernatant by UV–visible spectrophotometer.

2.5. Photocatalysis procedure

In a typical process, the catalytic reaction was carried out in a 100 ml photoreactor (Scheme 2), which contain 10 ml of MB dye (20 mg/l) solution and 6 mg of catalyst. Before the irradiation, the solution was stirred in the dark (15 min) to allow equilibrium of the system. Irradiation was carried out using 400 W tungsten and 400 W high pressure mercury lamps as the light sources. All photocatalytic experiments were carried out at the same conditions. The distance between photoreactor and light sources was 20 cm. Samples (3 ml) were collected during the irradiation and MB solution were separated from the photocatalyst by centrifugation. The degradation was monitored by measuring the absorbance amount using a double beam UV–vis spectrophotometer (Shimadzu UV-1700) at 664 nm wavelength.

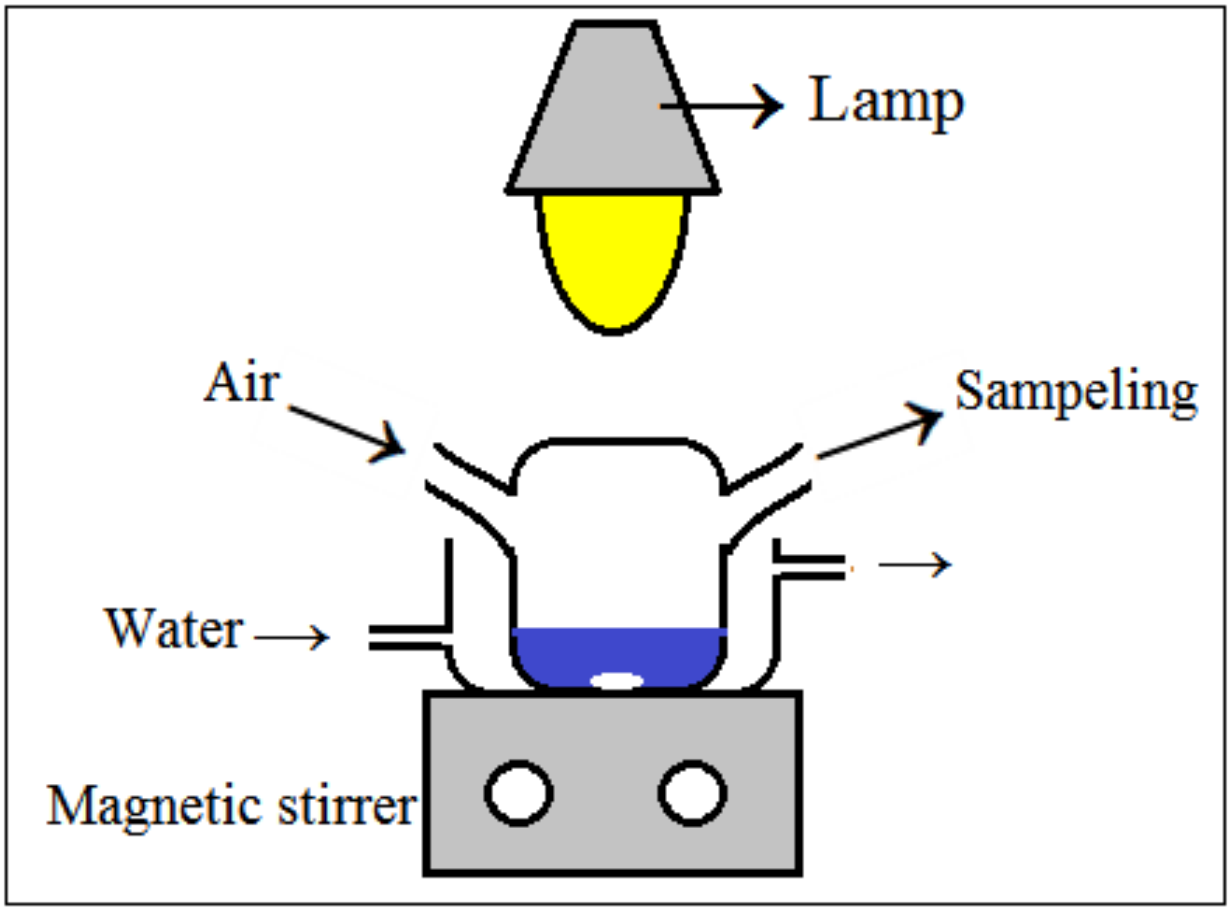

Scheme 2. Schematic representation of the photoreactor.

3. Results and discussion

3.1. Morphological characterizations

The morphology of the ZnO particle was examined from SEM images, as shown in Fig. 1. It was found that all synthesized ZnO nanorods were quite uniform in size. Fig. 1A,B show SEM images of the pure ZnO and Fig. 1C,D are related to TPPS/ZnO nanorods.

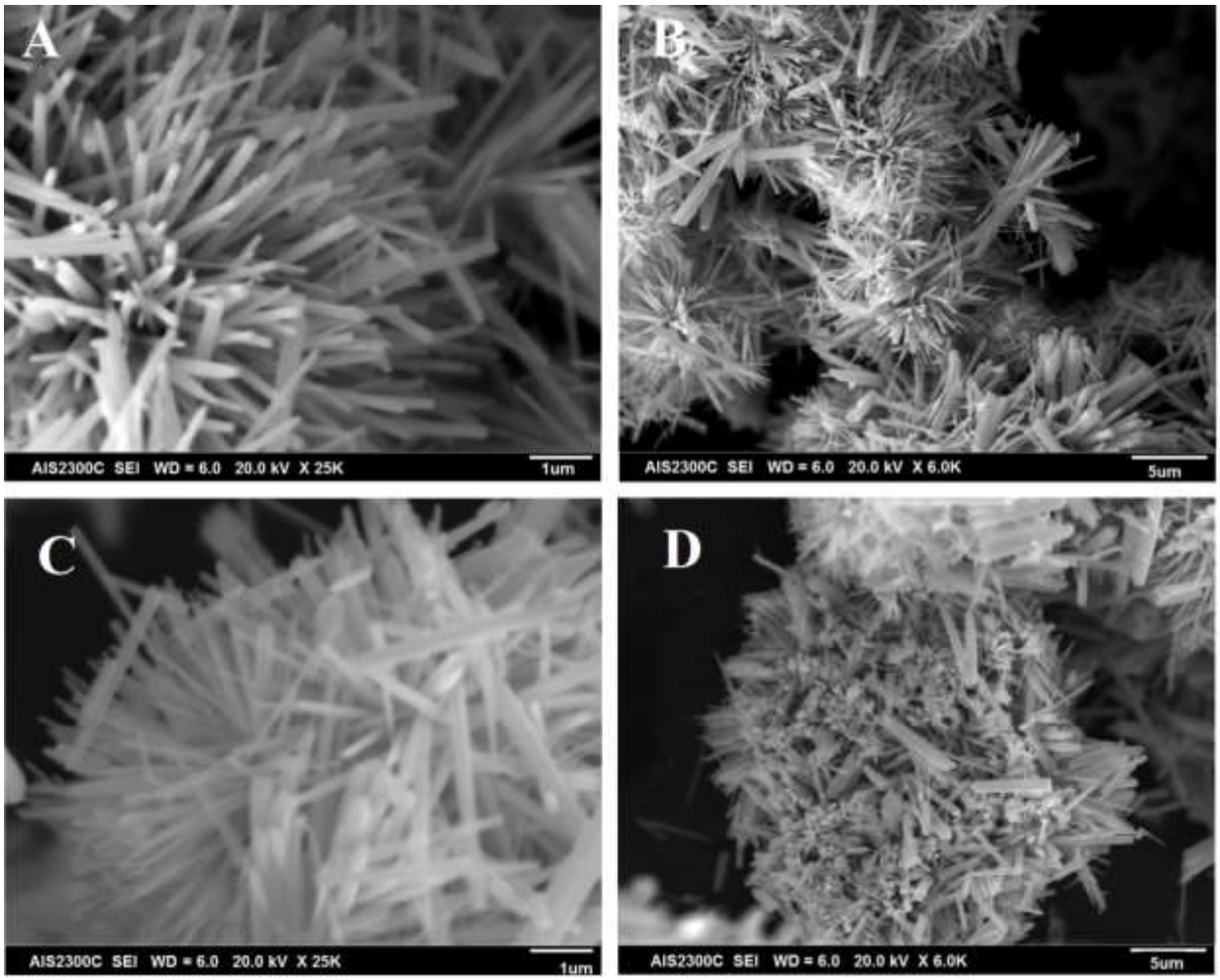

Fig. 1. The SEM images of the synthesized (A,B) ZnO and (B,C) TPPS/ZnO nanorods.

3.2. The X-ray powder diffraction

Fig. 2 shows the XRD pattern of ZnO nanorod powders. It can be seen that all these peaks are in good agreement with hexagonal (wurtzite) ZnO (JCPDS Card, No. 36-1451). Table 1 shows that the calculated d-values are in good agreement with those taken from the JCPDS card file data for ZnO powder. No peaks, any else phase of ZnO or impurity peaks are observed, which indicates the high purity of the obtained ZnO nanorods. [18]. On the whole, these diffraction peaks are sharp, narrow and symmetrical with a low and stable baseline, suggesting that the sample is well crystallized [19].

Table 1. The XRD parameters of (h k l), 2Θ and d-value of the Synthesized ZnO nanorods

h k l	Synthesized ZnO nanorods			JCPDS 36-1451		
	2Ɵ (degree)	d -Value (Å)	I (%)	2Ɵ (degree)	d -Value (Å)	I (%)
1 0 0	31.8194	2.81239	61.23	31.770	2.81430	57
0 0 2	34.4762	2.6015	54.61	34.422	2.60332	44
1 0 1	36.2973	2.47505	100	36.253	2.47592	100
1 0 2	47.5898	1.9108	19.69	47.539	1.91114	23
1 1 0	56.6653	1.62443	22.6	56.603	1.62472	32
1 0 3	62.9221	1.47712	21.67	62.864	1.47712	29
2 0 0	66.4036	1.40787	1.83	66.380	1.40715	4
1 1 2	67.9976	1.3787	15.89	67.963	1.37818	23
2 0 1	69.1258	1.35893	7.95	69.100	1.35825	11
0 0 4	72.6191	1.30193	1.78	72.562	1.30174	2
2 0 2	76.9981	1.23743	2.21	76.955	1.23801	4

The synthesized ZnO nanorods diameter was calculated using Debye-Scherrer formula.

$$d = \frac{0.89\lambda}{\beta \, Cos\theta}$$

Where 0.89 is Scherrer's constant, λ is the wavelength of X-rays, θ is the Bragg diffraction angle, and β is the full width at half-maximum (FWHM) of the diffraction peak corresponding to plane (101). The average particle size of the sample was found to be 21.05 nm which is derived from the FWHM of more intense peak corresponding to (1 0 1) plane located at 36.30◦ using this formula.

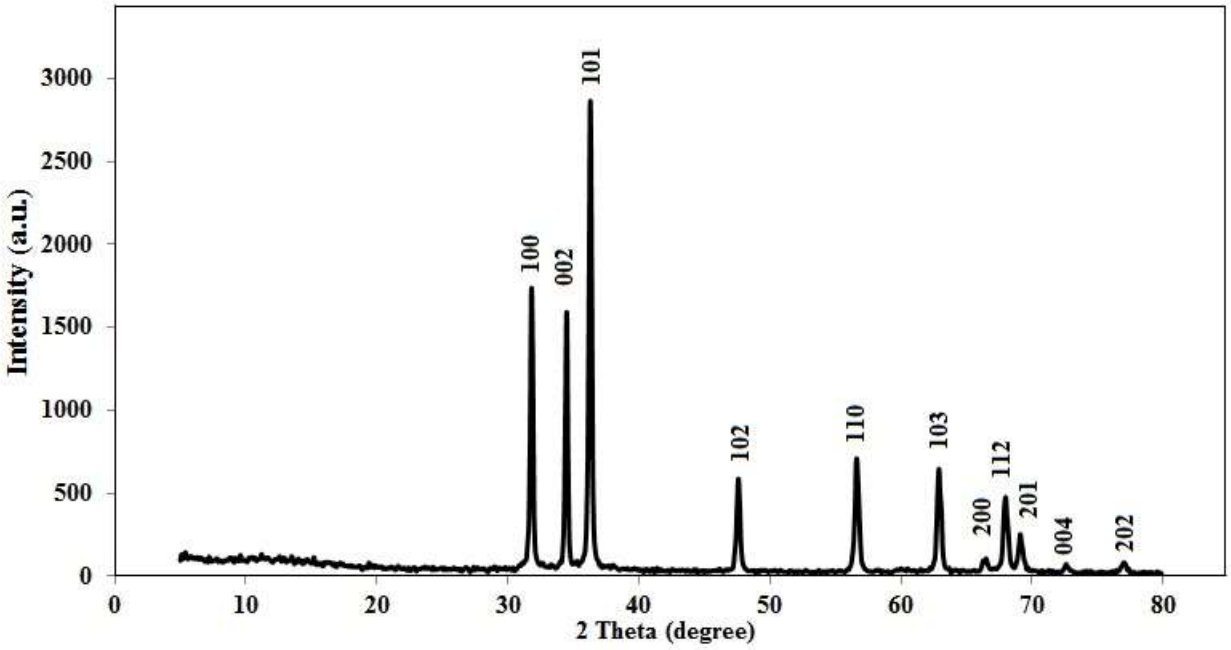

Fig. 2. The XRD pattern of the synthesized ZnO nanorods.

3.3. Optical properties

The UV–vis diffuse reflectance spectra (DRS) of the synthesized ZnO nanorods and TPPS/ZnO and the UV–vis spectrum of pure TPPS (in methanol) at room temperature are shown in Fig. 3A. The spectrum reveals a characteristic absorption peak of ZnO at wavelength of 368, which can be assigned to the intrinsic band-gap absorption of ZnO due to the electron transitions from the valence band to the conduction band ($O_{2p} \rightarrow Zn_{3d}$) [20].

In semiconductor, the absorption coefficient is a function of the incident photon energy. Near the absorption edge, the absorption coefficient for direct transition is given by [21]:

$$\alpha h\vartheta = A\left(h\nu - E_g\right)^n$$

where Eg (eV) is the energy gap, hν (eV) is the energy of incident photon and constant A varies for different transitions, and is related to effective mass of carriers, refractive index, oscillator strength and so on. The n is an index which equals 1/2 corresponding to allowed direct transitions [22].

The extrapolation method is usually used to determine the band gap of semiconductors providing that the transition in the semiconductor at certain wavelength scope is direct. In this work, when the index n is 1/2 in above Eq., by using the relationship of reflectivity and transmission with

wavelength, we calculated the square of the absorption coefficient as a function of the incident photon energy (as shown in Fig. 3B). The energy band gap Eg measurement is 3.23 eV.

The absorption range of the composite is wider in comparison with those of pure TPPS and ZnO nanoorods. The UV–visible spectrum of pure TPPS is containing a Soret peak in 413 nm and four Q peaks in 513, 553, 557 and 633 nm. Besides, the Soret and Q bands of the porphyrin of the composite are red-shifted related to those of the pure TPPS. Furthermore, the intensity ratio of Soret band to Q bands of the TPPS/ZnO is lower than that of the pure TPPS. Based upon these observations, it is demonstrated that the porphyrin has been assembled on the surface of ZnO nanorods, and there exists a strong interaction between ZnO nanorods and porphyrin in the TPPS/ZnO.

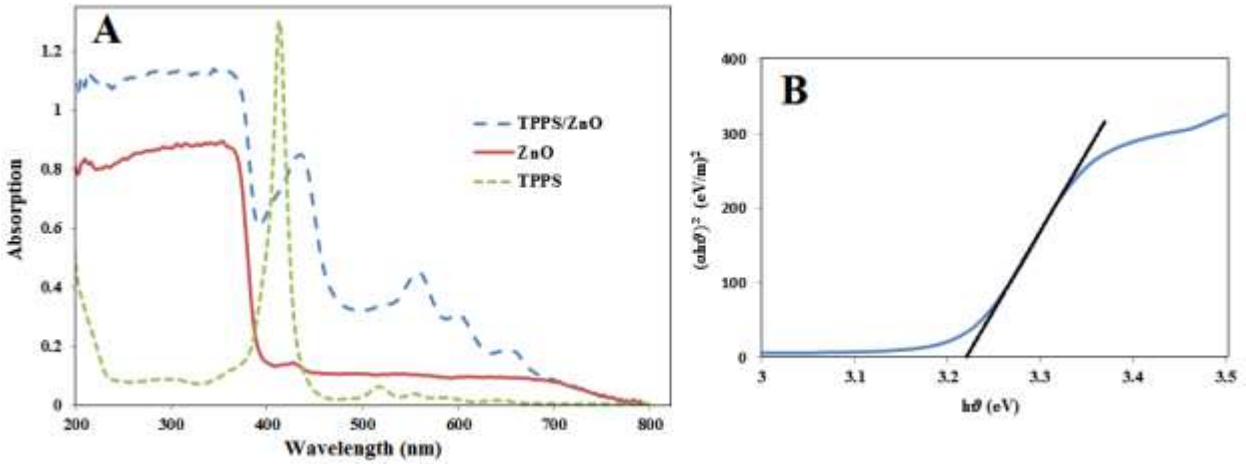

Fig. 3. (A) The diffuse reflectance spectra (DRS) of the synthesized ZnO, TPPS/ZnO and the UV–vis spectrum of pure TPPS (in methanol) and (B) the plot for band-gap energy (E_{bg}) of ZnO.

3.4. Fourier transforms infrared spectroscopy

Fig. 4 shows the FT-IR spectra of the ZnO nanorods, TPPS and the TPPS/ZnO measured in the range of 390–4000 cm^{-1}. The appearance of a sharp band at 401 and 501 cm^{-1} in the FT-IR spectra confirms the synthesis of ZnO because it is the characteristic absorption band for the Zn–O stretching vibration [23]. Additionally broad absorption peaks centered at around 3446 cm^{-1} is caused by the O–H stretching of the absorbed water molecules because the nanocrystalline materials exhibit a high surface to volume ratio.

For the FT-IR of TPPS, the stretching vibration of =C-N and –C=N bands (pyrrole) appeared at 1373 cm^{-1} and 1720 cm^{-1}, respectively. The stretching asymmetric and symmetric vibration bands attributed to the C-H (CH_2) band are discernible in 2846, 2918 and 2939 cm^{-1}. The appearance of the peaks at 890, 1100 and 3387 cm^{-1} could be attributed to C_6H_4 (phenyl), SO_3 group and N-H band, respectively.

For the FT-IR of TPPS/ZnO, the appearance of peaks corresponded to TPPS confirm that porphyrin have immobilized on ZnO nanorods but these peaks are difficult to give precise values because of very low intensities due to a low loading of the macrocycle into the inorganic matrix.

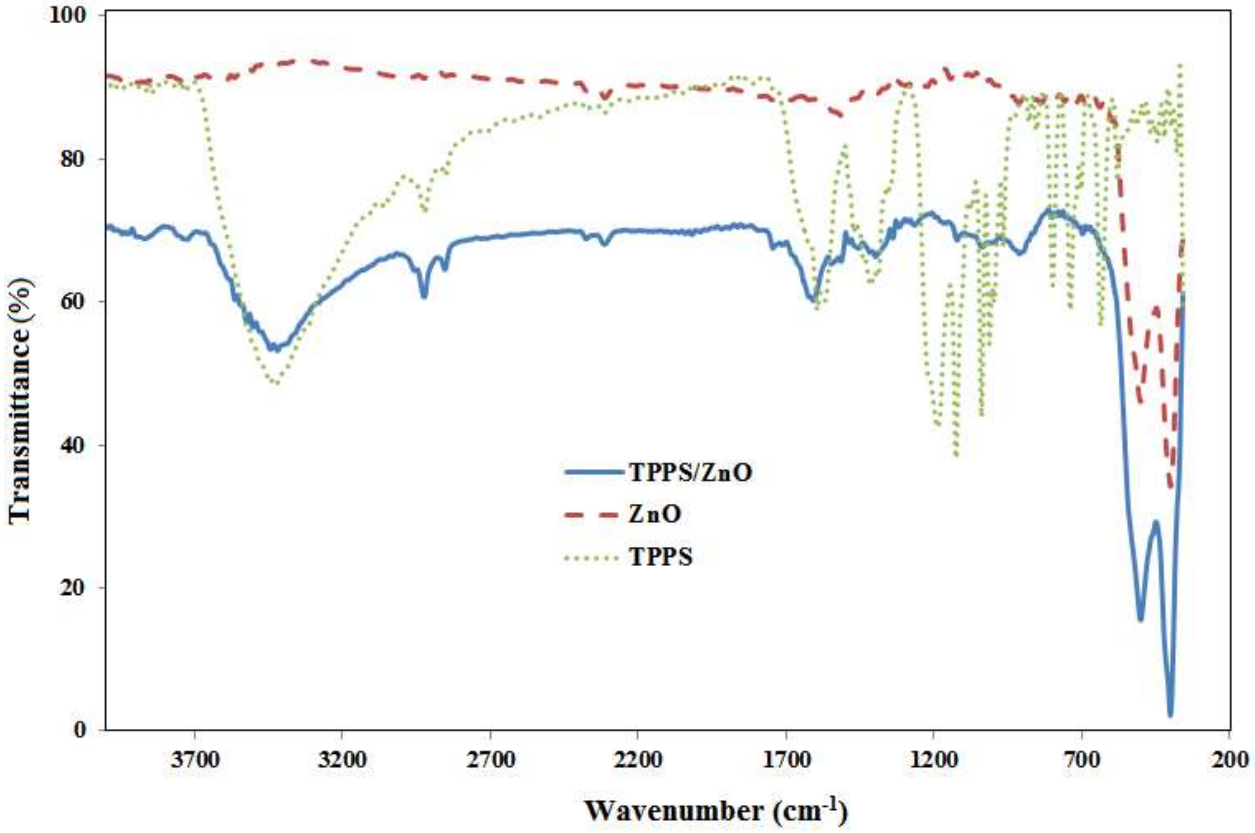

Fig. 4. The FT-IR spectrum of the synthesized ZnO, TPPS/ZnO and pure TPPS.

3.5. Photocatalytic degradation of methylene blue

The photocatalytic activities of as-synthesized two kinds of catalysts were evaluated by the degradation of organic dyes methylene blue in aqueous solution under light irradiation. The TPPS/ZnO nanorods and ZnO nanorods, with a high specific surface area, were used as

photocatalysts for the decomposition of methylene blue by the superoxides and/or hydroxyl radicals formed at their interface. The characteristic absorption of MB at 664 nm was chosen to monitor the photocatalytic degradation process. Concerning the initial MB concentration, it can be concluded that there was a decrease in the photodegradation of MB with increasing initial MB concentration. Fig. 5 shows a typical photocatalytic degradation process of MB (initial concentration:10 mg/l, 20 ml) using TPPS/ZnO (0.01 g) under visible light irradiation. The absorption peaks corresponding to MB diminished gradually as the exposure time was extended.

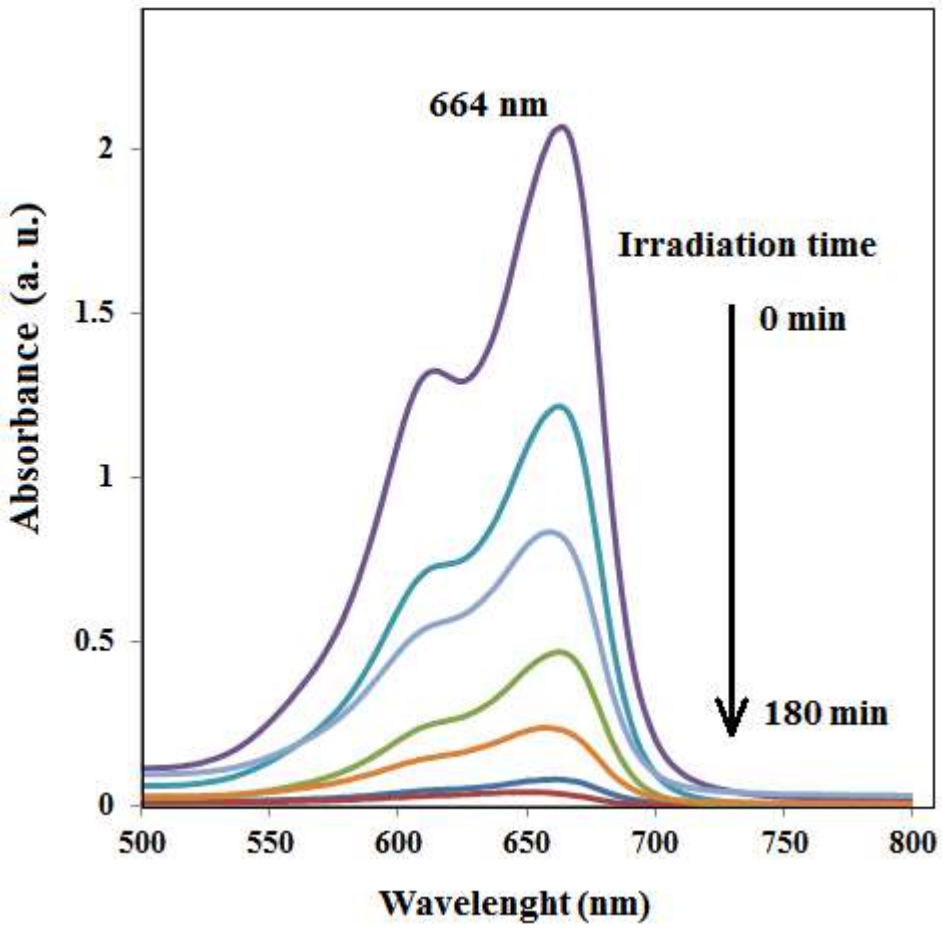

Fig. 5. The temporal evolution of the absorption spectra of the MB solution (initial concentration: 10 mg/l, 20 ml) in presence of TPPS/ZnO catalyst (0.01 g) under visible light irradiation.

Fig. 6 shows the photocatalytic efficiency of samples under visible and UV light irradiation. The best photodegradation of MB was carried using CuTCPP/ZnO under UV nd visibe light

irradiation (100%). After the ZnO nanorods is sensitized by porphyrin, higher photoactivity is obtained under visible light irradiation and porphyrin/ZnO shows the better catalytic property than that of ZnO nanorods. It indicates that porphyrin played different role in the photoreactivity process [16].

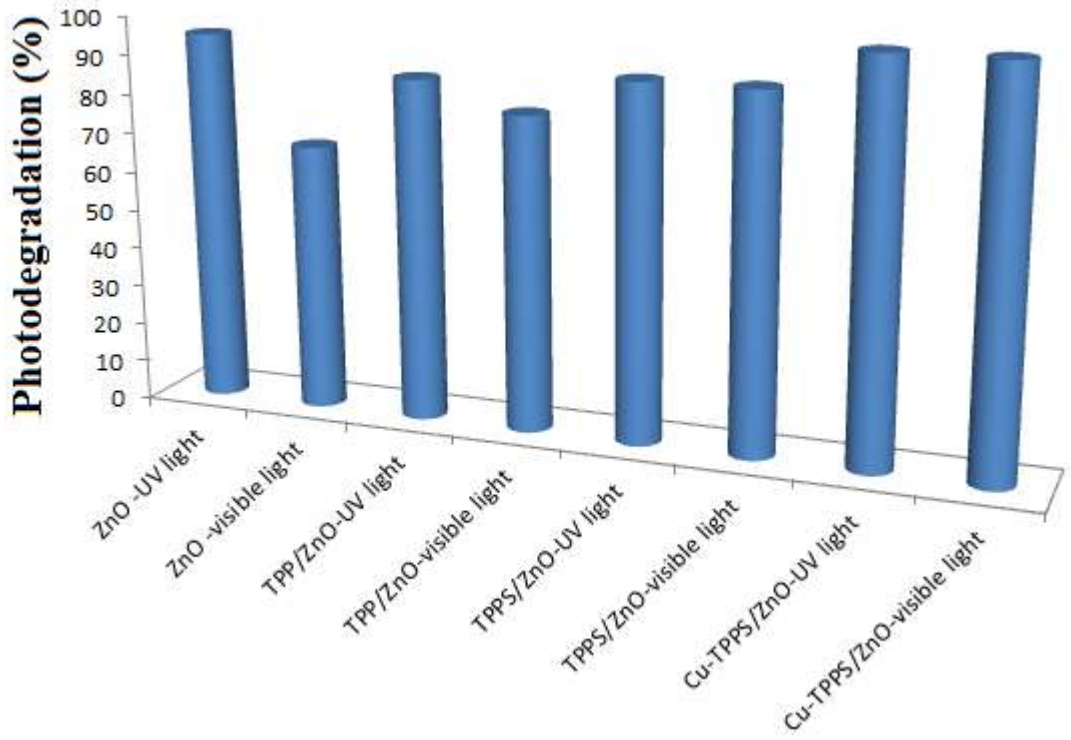

Fig. 6. Degradation efficiency of MB with different conditions under visible and UV light irradiation.

4. Conclusion

The photocatalytic degradation of MB in water was studied using ZnO and visible and UV light irradiation. The obtained results indicate that the photodegradation of MB was affected by the initial MB concentration and type of light irradiaton.

References

[1] K.W. Boer, C.P. Poole, J.P. Heremans, Survey of semiconductor physics, John Wiley & Sons New York, 2002.

[2] U. Ozgur, Y.I. Alivov, C. Liu, A. Teke, M. Reshchikov, S. Dogan, V. Avrutin, S.-J. Cho, H. Morkoc, A comprehensive review of ZnO materials and devices, Journal of applied physics, 98 (2005) 041301-041301-041103.

[3] A. Tsukazaki, A. Ohtomo, M. Kawasaki, High-mobility electronic transport in ZnO thin films, Applied physics letters, 88 (2006) 152106-152106-152103.

[4] C. Guillen, J. Herrero, High conductivity and transparent ZnO: Al films prepared at low temperature by DC and MF magnetron sputtering, Thin Solid Films, 515 (2006) 640-643.

[5] L.-H. Zhao, R. Zhang, J. Zhang, S.-Q. Sun, Synthesis and characterization of biocompatible ZnO nanoparticles, CrystEngComm, 14 (2012) 945-950.

[6] Y.-K. Su, S. Peng, L. Ji, C. Wu, W. Cheng, C. Liu, Ultraviolet ZnO nanorod photosensors, Langmuir, 26 (2009) 603-606.

[7] B.S. Ong, C. Li, Y. Li, Y. Wu, R. Loutfy, Stable, solution-processed, high-mobility ZnO thin-film transistors, Journal of the American Chemical Society, 129 (2007) 2750-2751.

[8] W. Shen, Z. Li, H. Wang, Y. Liu, Q. Guo, Y. Zhang, Photocatalytic degradation for methylene blue using zinc oxide prepared by codeposition and solâ€“gel methods, Journal of Hazardous Materials, 152 (2008) 172-175.

[9] L. Ghule, A. Patil, K. Sapnar, S. Dhole, K. Garadkar, Photocatalytic degradation of methyl orange using ZnO nanorods, Toxicological & Environmental Chemistry, 93 (2011) 623-634.

[10] D. Jian, P.-X. Gao, W. Cai, B.S. Allimi, S.P. Alpay, Y. Ding, Z.L. Wang, C. Brooks, Synthesis, characterization, and photocatalytic properties of ZnO/(La, Sr) CoO3 composite nanorod arrays, Journal of Materials Chemistry, 19 (2009) 970-975.

[11] M.R. Hoffmann, S.T. Martin, W. Choi, D.W. Bahnemann, Environmental applications of semiconductor photocatalysis, Chemical reviews, 95 (1995) 69-96.

[12] D. Mijin, M. Savić, P. Snežana, A. Smiljanić, O. Glavaški, M. Jovanović, S. Petrović, A study of the photocatalytic degradation of metamitron in ZnO water suspensions, Desalination, 249 (2009) 286-292.

[13] S. Chakrabarti, B.K. Dutta, Photocatalytic degradation of model textile dyes in wastewater using ZnO as semiconductor catalyst, Journal of Hazardous Materials, 112 (2004) 269-278.

[14] H. Wang, C. Xie, W. Zhang, S. Cai, Z. Yang, Y. Gui, Comparison of dye degradation efficiency using ZnO powders with various size scales, Journal of Hazardous materials, 141 (2007) 645-652.

[15] D. Li, H. Haneda, Morphologies of zinc oxide particles and their effects on photocatalysis, Chemosphere, 51 (2003) 129-137.
[16] C.A. Gouvea, F. Wypych, S.G. Moraes, N. Duran, N. Nagata, P. Peralta-Zamora, Semiconductor-assisted photocatalytic degradation of reactive dyes in aqueous solution, Chemosphere, 40 (2000) 433-440.
[17] W.-j. Sun, J. Li, G. Mele, Z.-q. Zhang, F.-x. Zhang, Enhanced photocatalytic degradation of rhodamine B by surface modification of ZnO with copper (II) porphyrin under both UVâ€“vis and visible light irradiation, Journal of Molecular Catalysis A: Chemical, 366 (2013) 84-91.
[18] W. Hu, S. Chen, B. Zhou, H. Wang, Facile synthesis of ZnO nanoparticles based on bacterial cellulose, Materials Science and Engineering: B, 170 (2010) 88-92.
[19] R. Wen, X. Fan, Z. Yang, Z. Tan, B. Yang, Electrochemical performances of ZnO with different morphology as anodic materials for Ni/Zn secondary batteries, Electrochimica Acta, (2012).
[20] A.K. Zak, M.E. Abrishami, W. Majid, R. Yousefi, S. Hosseini, Effects of annealing temperature on some structural and optical properties of ZnO nanoparticles prepared by a modified sol–gel combustion method, Ceramics International, 37 (2011) 393-398.
[21] S.M. Sze, K.K. Ng, Physics of semiconductor devices, Wiley. com, 2006.
[22] F. Li, C. Liu, Z. Ma, L. Zhao, New methods for determining the band gap behavior of ZnO, Optical Materials, 34 (2012) 1062-1066.
[23] A. Al-Hajry, A. Umar, Y. Hahn, D. Kim, Growth, properties and dye-sensitized solar cells–applications of ZnO nanorods grown by low-temperature solution process, Superlattices and Microstructures, 45 (2009) 529-534.
[24] J. Niu, B. Yao, Y. Chen, C. Peng, X. Yu, J. Zhang, G. Bai, Enhanced photocatalytic activity of nitrogen doped TiO_2 photocatalysts sensitized by metallo Co, Ni-porphyrins, Applied Surface Science, (2013).